

Multi-mission remote sensing of low concentration produced water slicks

A. Malin Johansson^a, Stine Skrunes^a, Camilla Brekke^a, and Hugo Isaksen^b

^aDepartment of Physics and Technology, UiT The Arctic University of Norway, 9037 Tromsø, Norway

^bKongsberg Satellite Services (KSAT), 9291 Tromsø, Norway

Abstract

Produced water is legally released from oil platforms and often detected by oil spill detection services despite their low oil concentrations. Using fully-polarimetric RADARSAT-2 and dual-polarimetric Sentinel-1 data we investigate their synthetic aperture radar (SAR) characteristics. Detectability ranges within the SAR and optical Sentinel-2 and PlanetScope images are assessed and compared to in-situ data from the Brage platform. Given similar release and environmental conditions are the detected slicks in optical images smaller and shorter than those observed in SAR images. The damping ratios and polarization differences are similar to thicker mineral oil slicks, though with higher within slick variance.

1 Introduction

Satellite Synthetic Aperture Radar (SAR) is the backbone for operational ocean surveillance and oil spill detection services. Though separation between actionable thicker oil spills, legal releases of produced water (PW) and other low backscatter phenomena is challenging. PW is a by-product in the oil and gas industry and consists largely of water, but contain also low concentrations of oil. Provided that the monthly average oil concentration is below 30 g/m^3 [1] it is legal to release the PW into the ocean, where it often forms thin surface slicks. From Norwegian oil platforms the monthly average oil concentration in the PW releases is 11.2 g/m^3 , and this is the largest source of legal released oil on the Norwegian shelf [2]. These legal releases are often detected close to oil platforms in the North Sea by operational oil spill detection services [3], and it is difficult to separate normal discharges from accidental larger releases of oil, or in case of an incident in the vicinity of the oil platforms. This may lead operators to overlook actionable oil spills close to platforms. Successful separation between the low concentration and high concentration oil slicks can also be used in tactical clean-up stages of an oil spill incident, by identifying areas with a larger relative thickness. State of the art remote sensing techniques for oil spill monitoring and detection are described in, e.g., [4]. Characterization of oil slicks in SAR images has been ongoing for decades, e.g., [5] and references therein, accurate detection algorithms has been developed using machine learning methods, e.g., [6] and the most suitable polarimetric SAR features and their false alarm rates has been investigated by, e.g., [7]. Studies combining SAR and optical satellite images for detection and characterisation of oil slicks are not as common, though, e.g., [8, 9] have found that the oil slick thickness required to generate a detection in optical images is higher than that required to trigger a detection in SAR

images. In [8] they found that continuous releases of oil will result in a more varying oil slick as weathering and advection will affect the already released oil, and at the same time there is a continuous release of new oil. Within optical images good contrast between slicks of different thickness has been identified and is used within the Bonn Agreement Oil Appearance Code (BAOAC) [10], and [11] showed different response in optical images based on the oil volume percentage. A combination of the two sensor types may therefore be beneficial. Studies investigating PW slicks using remote sensing are limited, e.g., [3, 12, 13, 14], and a study using a combination of SAR and optical images has to the authors knowledge not been attempted before.

The aims of this work are to; i) investigate the PW release conditions needed to generate a detection in optical and SAR images, ii) compare the SAR and optical signatures acquired under the same PW release conditions, iii) investigate the C-band SAR characteristics of PW using a large set of Sentinel-1 (S-1) and RADARSAT-2 (RS-2) images, and iv) to compare with SAR signatures from higher concentration and higher volume releases during the oil-on-water (OOW) exercises in 2012 and 2013 [15].

2 Data set

PW is legally released into the North Sea from the platform Brage (60.5425°N , 3.0468°E) at 17 m below the surface. There is a time difference between the SAR and the optical image acquisitions of $\sim 5 \text{ h}$. Wind, waves and currents affect the oil slick thickness and distribution, and drift and weathering processes will change the oil properties over time. A pixel to pixel comparison between the optical and SAR images are therefore not possible. However, the in-situ information is collected daily at the platform and the analysis can therefore be carried out comparing the slick size, length and observations related to the PW releases.

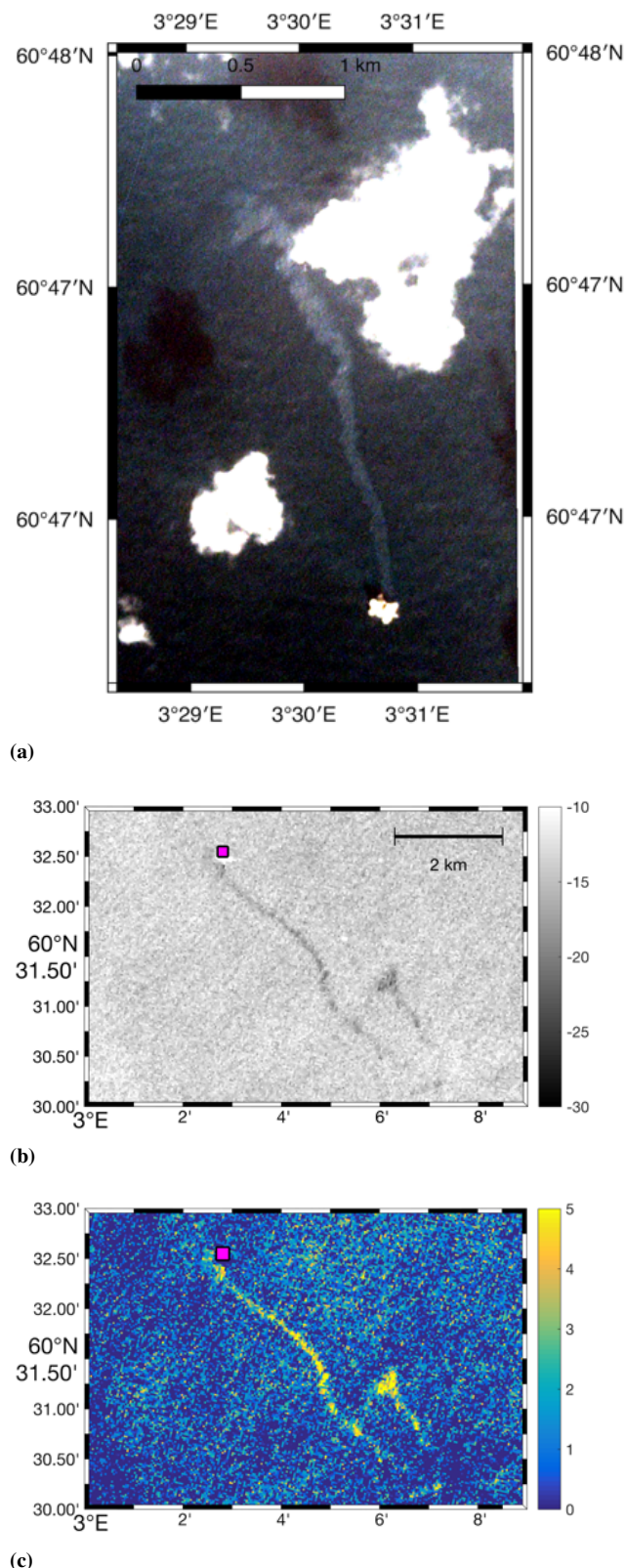


Figure 1 The optical and SAR image pair from 14.08.2019, where a) is a PlanetScope scene in true color image (red, green and blue bands) acquired at 10:41 UTC, and b) is a RS-2 VV intensity image in dB acquired at 06:18 UTC. In c) the DR, in dB, for the RS-2 image is shown. The Brage platform is seen in the lower centre of the PlanetScope scene, and indicated by a magenta square in the RS-2 image. Note the change in slick direction between the two images.

2.1 Satellite data

All available overlapping optical Sentinel-2 (S-2) images from 2018 (130) and 2019 (131) were included in the analysis, as well as 15 PlanetScope images. The spatial resolutions are 3 m for PlanetScope and 10 m for S-2. The S-2 images were first analysed for cloud-free conditions, and the remaining 30 (2018) and 40 (2019) images were further analysed for presence of oil slick. Out of the total number of optical images 8 overlap in space and time with the RS-2 images. In total were 32 RS-2 images collected between May and September in 2018 and 2020. The RS-2 images were acquired in quad-polarization mode, with a pixel spacing of 5.1 m (range) and 7.6 m (azimuth), and with modes FQ8 (Incidence angle (IA) $\sim 27^\circ$) and FQ10 (IA $\sim 30^\circ$), thereby reducing differences in the satellite configuration. Two RS-2 images collected over the yearly OOW exercise in 2012 and 2013 with similar IAs, FQ9 and FQ11, are included in the analysis and represent comparatively thicker oil slicks [15]. In total, were 189 (2018) and 167 (2019) S-1 images analysed for presence of slicks. The S-1 images were collected in Interferometric Wide (IW) Ground Range Detected (GRD) mode (VV/VH), and has a pixel spacing of 10×10 m. The four pre-set orbits meant that the platform is located at four different IAs, $\sim 32^\circ$, $\sim 37^\circ$, $\sim 39^\circ$ and $\sim 44^\circ$ within these scenes. In Figure 1 one PlanetScope scene (10:41 UTC) and one RS-2 image (06:18 UTC) from the 14.08.2019 are shown.

2.2 In-situ data

Meteorological data is recorded every 10 minutes at the Brage platform, and the wind measurements closest in time for each of the satellite images is used. Information about the PW releases is routinely recorded at the platform and here we utilise the mean daily concentrations (g/m^3), the hourly discharge volumes (m^3) and the mean daily released oil mass (kg). There may not be a continuous PW release and the release is at times stopped completely. The use of mean daily information is adhered with some uncertainty as the slick may only consist of PW from a more limited time period, as it may have dispersed during the day. Data with higher temporal frequency was used in [12] and show relatively small variations in one day. We therefore hypothesise that the mean daily values are representative of the release conditions during the day. The daily mean hourly PW discharge volumes lies between 230 and 1060 m^3 with the oil component being $0.003\text{--}0.018 \text{ m}^3$. The mean daily concentration is $56 \text{ g}/\text{m}^3$ or lower (Figure 2), though note that a high oil concentration does not necessarily correspond to a high discharge volume.

3 Method

The slick areas within the S-1 and RS-2 images are extracted using the segmentation algorithm presented in [16]. True color images using bands 2–4 (S-2) and red, green and blue (PlanetScope) were used to identify slicks within the optical images, and region of interests (ROIs) were manually identified. The length of the slick ($Length_{\text{slick}}$)

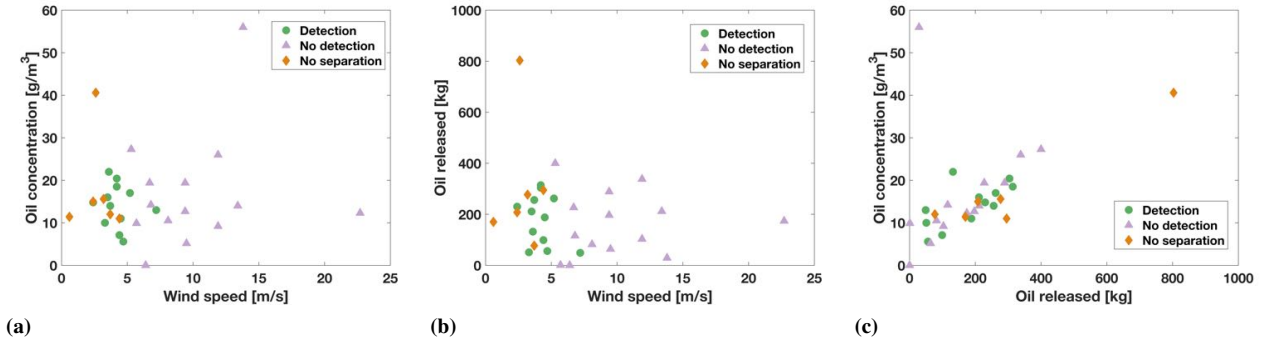


Figure 2 PW slick observations within the RS-2 images are plotted against the oil concentration (g/m^3) (a), oil release (kg) (b) and the wind speed (m/s) at the time of the satellite acquisition, with detection (green dots), no detection (purple triangles) and no separations (orange diamonds) indicated. In (c) is the mean daily oil concentration plotted against the mean daily oil release discharge.

is defined as the longest continuous distance between the platform and the end of the slick including the curvature of the slick and is manually identified. The distance ($Length_{Bragg}$) is the straight line distance from the platform to the end of the slick excluding the curvature.

3.1 SAR parameters

For the S-1 and RS-2 images are the backscatter intensity values and the damping ratio (DR) extracted, and for the RS-2 data the polarization difference (PD). The low backscatter phenomenon studied here means that the backscatter intensity values from co-polarization channels are favoured due to their inherently better signal to noise ratio (SNR) compared to the cross-polarization channels. Though for the S-1 images is only one of the co-polarization channels provided with each image. For consistency between the two SAR sensors, and the fact that the vertical transmit and receive polarization (VV) (co-polarization) channel is routinely used for oil spill detection, we use this channel expressed as:

$$\sigma_{VV}^0 = 10 \log_{10} \langle |S_{VV}|^2 \rangle \quad (1)$$

where $\langle |S_{VV}|^2 \rangle$ is the mean intensity of the complex scattering coefficient S . The RS-2 images are multi-looked using a 4×8 pixels window to reduce speckle, no additional multi-looked is performed on the S-1 images.

A commonly used oil-sea contrast measure is the DR (Figure 1c) and work by e.g., [17], suggest that there is a relationship between the oil slick thickness and the DR . A distinct advantage of this feature is that it can be estimated using only one channel. The DR is defined as;

$$DR = \frac{\langle |S_{VV}|^2 \rangle_{sea}}{\langle |S_{VV}|^2 \rangle_{slick}}, \quad (2)$$

The DR is calculated using open water pixels (sea) adjacent to the slick from the exact same incidence angle as the slick pixels ($slick$). The open water mean is averaged over 150 azimuth pixels at each position.

PD (Eq. 3) has been shown to provide good oil detection results in e.g. [7, 18, 19], and to be less sensitive to inci-

dence angle variations compared to e.g. the co-polarization ratio and to be less sensitive to additive noise [20].

$$PD = \langle |S_{VV}|^2 \rangle - \langle |S_{HH}|^2 \rangle. \quad (3)$$

where $\langle |S_{HH}|^2 \rangle$ is the mean intensity of the complex scattering coefficient S for the horizontal transmit and receive polarization (HH).

To quantify the spatial texture heterogeneity within the slicks the coefficient of variation (CV) is calculated for each of the two different parameters. CV is defined as;

$$CV = \sigma_X / \mu_X. \quad (4)$$

where σ_X is the standard deviation and μ_X is the mean value of the respective feature.

The S-1 signal to noise ratio (SNR) median lies between -2 and 16 dB and mostly around 5.0 dB, though only 10 images fulfill the $SNR > 10$ dB criteria [20]. For the RS-2 data the median SNR lies between 6.9–22.4 dB and all but one images has mean $SNR > 10$ dB. From this we can expect the S-1 backscatter values to be affected by the closeness to the noise floor, and this should be considered for any detailed scattering analysis. Though here all images are included regardless of SNR. The RS-2 values are less affected, partially as a consequence of the lower IAs for the RS-2 images acquired compared to the S-1 images.

4 Results and discussion

We observe that even low oil concentrations ($5\text{--}56 \text{ g/m}^3$) produce clearly detectable slicks in both the SAR and optical images. Out of the original set of 356 S-1 images PW slicks were identified in 76 images (2018) and 85 images (2019) respectively. Within the SAR images there are three types of observations; detection, no detection and no separation from the surrounding open water. For the optical images there were only detection or no detection.

4.1 Comparison of SAR and optical results

Due to the inherent differences in the satellite orbital paths no temporal overlap with < 5 h separation between the two

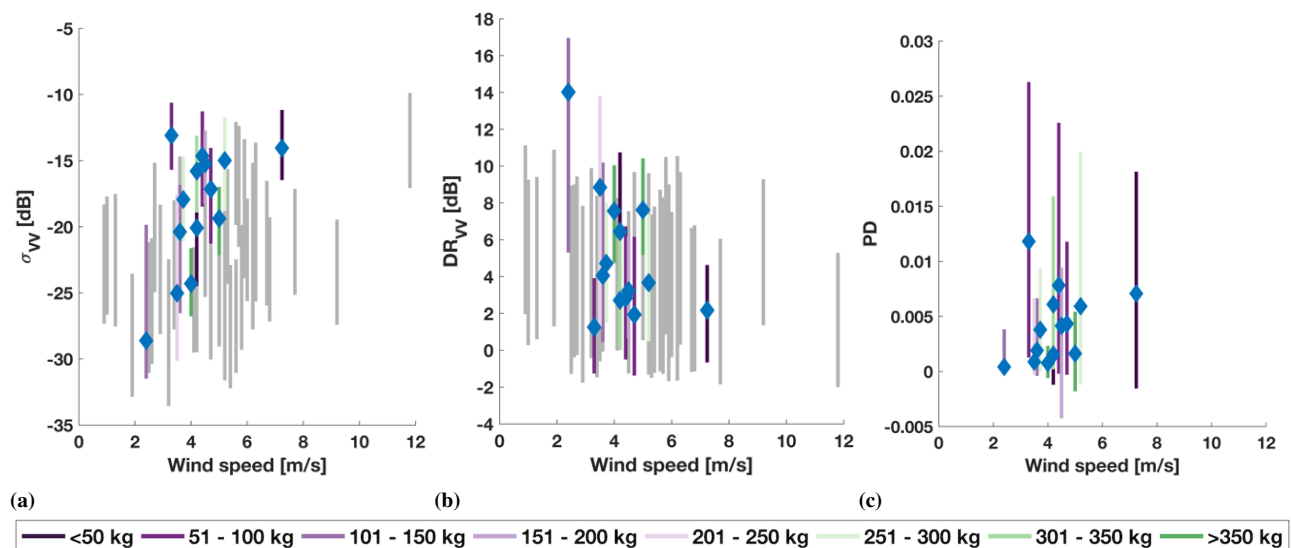


Figure 3 SAR derived parameters for the PW slick vs wind speed (m/s) at the time of the SAR acquisition, (a) backscatter intensity, (b) DR and (c) PD . The S-1 images are shown as grey lines and the colour coding for the RS-2 is based on the released amount of oil (kg) at the time of the satellite image acquisition. The lines indicate the range from the 5th percentile to the 95th percentile, and for the RS-2 is the mean value indicated with a diamond.

different types of satellite sensors is possible. The comparison is therefore conducted using slick observations from comparable PW oil concentration and release volume, and environmental conditions. Assuming a slick drift speed of 3% of the wind velocity [21] measured on the same day as the slick was observed and the measured slick length we observe that the estimated mean age of the slicks is 22.6 h for the S-1 images and 16.4 h for the S-2 images. Implying that a comparison with the mean daily release information should be applicable. Slicks were observed for wind speeds ranging from 1–13 m/s (optical) and from 1–12 m/s (SAR), with reduced separation for wind speeds <4.5 m/s in the SAR images (Figure 3). Similar to [12], where PW slicks were detected for wind speeds 2–12 m/s with reduced detectability above 9 m/s, and lies within the theoretically defined oil spill detection range of 2–14 m/s [22]. Moreover, it agrees with the optimal detection range (0.3–8.3 m/s) for optical image from [23]. The PW slicks were observed at discharge water volumes from 6500 m³ in the S-2 images, and from 10000 m³ in the S-1 images. This difference might be related to the lower wind speeds for the S-2 images (2–4 m/s) compared to the S-1 images (5–9 m/s) for the same lower discharge volumes. Though could indicate that PW slicks are observable in optical images under lower release volumes than in the SAR images. A noted difference between the observations in the SAR and optical images are the difference in slick length and area. Within the S-2 images are the mean $Length_{slick} \sim 4.3$ km (2018) and ~ 3.2 km (2019), which is shorter than those detected within the SAR images, ~ 7.2 km (2018) and ~ 8.1 km (2019). The longest $Length_{Bragg}$ were in the S-1 data 21.0 km (2018) and 34.6 km (2019). Normalised histograms for the different $Length_{slick}$ for

the S-1 and S-2 data are shown in Figure 4. The mean $Length_{slick}$ in the PlanetScope image is ~ 2.1 km, and in the RS-2 images ~ 4 km. The mean slicks size within all the S-1 images were 1.66 km² (2018) and 1.54 km² (2019) and within the S-2 images 0.45 km² (2018) and 0.25 km² (2019).

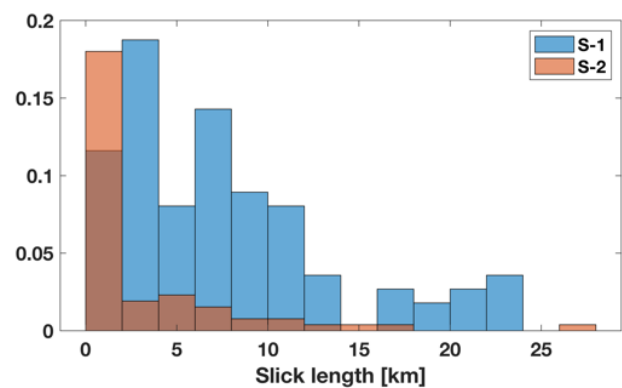


Figure 4 Normalised histogram of $Length_{slick}$ for the S-1 (blue) and S-2 images (orange).

The larger areas observed in SAR compared to optical images are in agreement with the results reported in, e.g., [8, 9]. In [8] they showed that the thinnest part of the oil slicks were only observed within the SAR images, and using temporally and spatially overlapping SAR and optical images [9] found that slick with thicknesses less than 1 μ m were not observed within the optical images, but thicknesses of $\sim 250 \mu$ m were clearly observed in both. In the optical images were the PW slicks classified as sheen, and according to BAOAC [10] the slick would then have a thickness of 0.04–0.30 μ m. Placing the PW slicks towards

the lower range of the observed thicknesses in [9]. That PW slicks with such low concentrations are clearly observable despite their potential thin thickness and low oil concentration means optical images under cloud free conditions can contribute valuable information for ocean surveillance, as distinction between thicker (actionable) and thinner (non-actionable) slicks may be possible. Moreover, the time difference means that optical images can contribute to a denser data set under cloud free conditions and potentially enable easier separation between PW slicks and biogenic slicks, where the latter is a well known look-alike in SAR images, e.g., [5] and references therein, but is easier to separate in optical images.

4.2 Slick variability

The variability within the detected oil slicks in the SAR images can be seen in Figure 3, where the wind speeds are shown together with the intensity (a), damping ratios (b) and (c) PD . For both sensors there is an increase in the intensity values with increasing wind speed, whilst the DR have a slight decrease. For the RS-2 data we observe DR values ranging from 2–14 dB, comparable to those observed in TerraSAR-X images (3–9 dB) in [12] for PW slicks, and within the same range as those observed over mineral oil slicks in [19]. The DR values for the S-1 images are slightly lower, ranging from 1–7 dB, though are consistent with the RS-2 values for the lowest IA (32°), indicating a good agreement between the two. The lower damping ratios at higher wind speeds is consistent with results in [13]. The lowest intensity values are also slightly higher for the S-1 images compared to the RS-2 images, possibly a consequence of the lower SNR in the S-1 data. The slicks observed in S-2 images showed limited observable internal variations, though two images acquired on 26.07.2018 and 29.07.2019 had clear variations. This is surprising as PW slicks are not generally considered to have thicknesses large enough to cause internal variations. It was hypothesised in [12] that the oil concentration in the PW slicks may be elevated at the ocean surface, compared to the released concentrations at 17 m depth, due to accumulation, possibly explaining the variability. Both images are within the lower range of the measured oil concentration, 12.0 and 10.4 g/m^3 respectively, though have reasonably different released volume, 6428 m^3 and 17774 m^3 respectively. Common for both where the very low wind speeds under which they were observed, 2.1 m/s and 1.7 m/s, potentially indicating that the observable internal variations in S-2 images are governed by the wind speed. Dependence on wind speed for internal variations were also observed in the S-1 images, where a slight increase in damping ratio variability (CV_{DR}) with increased wind speed and a corresponding decrease in $CV_{\sigma_{VV}^0}$, see Table 1. The variability in the backscatter and DR values containing the PW slicks are comparable for the S-1 and RS-2 images. Different thicknesses affect the SAR signal and work by e.g. [17] have all investigated the relative change in the DR related to oil slick thicknesses. The decreased damping ratio with increased wind speed may therefore indicate a thinning of the oil and the increased

variability a more spread out oil slick.

Table 1 CV for σ_{VV}^0 and DR . The RS-2 CV values at the top are average values for the two different beams, FQ8 ($\sim 27^\circ$) and FQ10 ($\sim 30^\circ$). The S-1 values are given as one average value for each different mean IA. The two OOW slicks are from the exercises in 2012 and 2013 and represent single scenes.

Sensor	IA	Type	$CV_{\sigma_{VV}^0}$	CV_{DR}
RS-2	$\sim 27^\circ$	PW	-0.12	0.52
RS-2	$\sim 30^\circ$	PW	-0.12	0.50
S-1	$\sim 32^\circ$	PW	-0.14	0.67
S-1	$\sim 37^\circ$	PW	-0.12	0.71
S-1	$\sim 39^\circ$	PW	-0.11	0.81
S-1	$\sim 44^\circ$	PW	-0.12	0.75
RS-2	$\sim 31^\circ$	OOW	-0.06	0.20
RS-2	$\sim 29^\circ$	OOW	-0.08	0.20

4.3 Comparison to higher concentration releases

Compared to higher concentration releases (OOW) is there a higher within slick variance for the PW releases for both σ_{VV}^0 and DR , yet the σ_{VV}^0 and DR values are comparable under the same wind conditions (>350 kg lines in Figure 3). The OOW data show CV values consistent with those observed for the persistent crude oil slick in MC-20 [24]. Both MC-20 and the observed PW slicks are near continuous releases though have very different oil concentrations. From this we hypothesise that separation between PW slicks and thicker mineral oil slicks may not be possible based on mono-polarization SAR features using S-1 images. However, the SNR for the S-1 images are below the recommended 10 dB limit and a system with an improved SNR may enable some separation. Moreover, the higher variability in the PW releases compared to the OOW and MC-20 data could possibly indicate that higher concentration oil releases can be separated from lower concentration PW releases through the within slick variability.

5 Conclusions

We investigate the SAR characteristics of PW slicks using 32 RS-2 and 161 S-1 images, and compare those findings with those of 70 optical S-2 and 15 PlanetScope images. Oil slicks were clearly observed in both types of sensor images for low oil concentrations (5–56 g/m^3) and low discharge volumes (>6500 m^3), and within slick variations were observed. PW slicks were observed during wind conditions from 1–12 m/s (SAR) and 1–13 m/s (optical). Damping ratios of 2–14 dB were estimated based on the SAR data, and are comparable to those observed for thicker oil slicks from the OOW exercises. However, the within slick variance was found to be larger in the PW slicks. Slicks were found to extend up to ~ 35 km away from the platform, though under similar PW releases and wind conditions were the slick size and length smaller in

the optical images compared to the SAR images. This is likely a result of thinner areas not being possible to observe in the optical images. Though the fact that slicks were observed in all optical images with wind speeds below 13 m/s, indicates that optical images can provide complementary information for operational monitoring.

6 Acknowledgement

The authors thank Wintershall for carrying out the in-situ data collection. RADARSAT-2 data was provided by NSC/KSAT under the Norwegian-Canadian Radarsat agreement (2012–13 and 2018–20). PlanetScope data provided by KSAT © PlanetScope. Copernicus Sentinel-1 and Sentinel-2 data 2018–2019 was processed by ESA. The work was funded by the Research Council of Norway through OIBSAR (#280616) and CIRFA (#237906).

7 Literature

- [1] OSPAR Recommendation 2001/1 for the management of produced water from offshore installations. url: <https://www.ospar.org/documents?d=32591>, OSPAR commission, 2001.
- [2] Miljørapport, Olje- og gassindustriens miljøarbeid, Fakta og utviklingstrekk. Technical report, Norsk olje & gass, 2019.
- [3] Singha, S., Velotto, D., Lehner, S.: Near real time monitoring of platform sourced pollution using TerraSAR-X over the North Sea. *Mar. Poll. Bull.*, 2014, vol. 86, pp. 379–390.
- [4] Fingas, M., Brown, C.: A review of oil spill remote sensing. *Sensors*, 2018, vol. 18, No. 2, p. 91.
- [5] Alpers, W., Holt, B. Zeng, K.: Oil spill detection by imaging radars: challenges and pitfalls. *Rem. Sens. Env.*, 2017, vol. 201, pp. 133–147.
- [6] Garcia-Pineda, O., MacDonald, I., Li, X., Jackson, C., Pichel, W.: Oil spill mapping and measurement in the Gulf of Mexico with textural classifier neural network algorithm (TCNNA). *IEEE JSTARS*, 2013, vol. 6, pp. 2517–2525.
- [7] Angelliaume, S., Dubois-Fernandez, P. C., Jones, C. E., Holt, B., Minchew, B., Amri, E., Miegbielle, V.: SAR Imagery for Detecting Sea Surface Slicks: Performance Assessment of Polarization-Dependent Parameters. *IEEE TGRS*, 2018, vol. 56, pp. 4237–4257.
- [8] Svejksky, J., Hess, M., Muskat, J., Nedwed, T., McCall, J., Garcia-Pineda, O.: Characterization of surface oil thickness distribution patterns observed during the deepwater horizon (MC-252) oil spill with aerial and satellite remote sensing. *Mar. Poll. Bull.*, 2016, vol. 110, pp. 162–176.
- [9] Brekke, C., Espeseth, M. M., Dagestad, K.-F., Röhrs, J., Hole, L., Reigber, A.: Integrated analysis of multi-sensor datasets and oil drift simulations - a free floating experiment in the open ocean. *JGR: Oceans*, 2020.
- [10] Bonn Agreement: Bonn agreement aerial surveillance handbook (pp.106). 2017.
- [11] Lu, Y., Shi, J., Hu, C., Zhang, M., Sun, S., Liu, Y.: Optical interpretation of oil emulsions in the ocean – Part II: Applications to multi-band coarse-resolution imagery. *Rem. Sens. Env.*, 2020, vol. 242, no.111778.
- [12] Skrunes, S., Johansson, A. M., Brekke, C.: Synthetic Aperture Radar Remote Sensing of Operational Platform Produced Water Releases, *Rem. Sens.* 2019, vol. 11, no. 23, pp. 2882.
- [13] Espedal, H., Johannessen, O. Johannessen, J., Dano, E., Lyzenga, D., Knulst, J.: Coastwatch'95: ERS 1/2 SAR detection of natural film on the ocean surface. *JGR: Oceans*, 1998, vol. 103, no. C11, pp. 24969–24982.
- [14] Espedal H., Wahl, T.: Satellite SAR oil spill detection using wind history information. *Int. J. Rem. Sens.*, 1999, vol. 20, no. 1, pp. 49–65.
- [15] Skrunes, S., Brekke, C., Eltoft, T., Kudryavtsev, V.: Comparing near coincident C- and X-band SAR acquisitions of marine oil spills. *IEEE TGRS*, 2015, vol. 53, no. 4, pp. 958–1975.
- [16] Cristea, A., Van Houtte, J., Doulgeris, A. P.: Integrating Incidence Angle Dependencies into the Clustering-Based Segmentation of SAR Images. *IEEE JSTARS*, 2020, vol. 13, pp. 2925–2939.
- [17] Sergievskaya, I., Ermakov, S., Lazareva, T., Guo, J.: Damping of surface waves due to crude oil/oil emulsion films on water. *Mar. Poll. Bull.*, 2019, vol. 146, pp. 206–214.
- [18] Kudryavtsev, V., Chapron, B., Myasoedov, A., Colard, F., Johannessen, J.: On Dual Co-Polarized SAR Measurements of the Ocean Surface. *IEEE GRSL*, 2013, vol. 10, pp. 761–765.
- [19] Skrunes, S., Brekke, C., Jones, C. E., Espeseth, M. M., Holt, B.: Effect of wind direction and incidence angle on polarimetric SAR observations of slicked and unslicked sea surfaces. *Rem. Sens. Env.*, 2018, vol. 213, pp. 73–91.
- [20] Espeseth, M. M., Brekke, C., Jones, C. E., Holt, B., Freeman, A.: The impact of system noise in polarimetric SAR imagery on oil spill observations. *IEEE TGRS*, 2020, vol. 58, pp. 4194–4214.
- [21] Drivdal, M., Broström, G., Christensen, K.: Wave-induced mixing and transport of buoyant particles: Application to the Statfjord A oil spill. *Ocean Sci.*, 2014, vol. 10, pp. 977–991.
- [22] Alpers W., Hühnerfuss, H.: The damping of ocean waves by surface films: A new look at an old problem. *JGR: Oceans*, 1989, vol. 94, pp. 6251–6265.
- [23] Sun, S., Hu, C: Sun glint requirement for the remote detection of surface oil films. *GRL*, 2016, vol. 43, pp. 309–316
- [24] A.M. Johansson, Espeseth, M.M. Brekke, C. Holt, B.: Can mineral oil slicks be distinguished from newly formed sea ice using synthetic aperture radar? *IEEE JSTARS*, 2020, vol. 13, pp. 4996–5010.